PHYSICAL METALLURGY AND HEAT TREATMENT

Investigations on the Effect of Cyclic Heat Treatment on the Mechanical Properties of Friction Stir Welded Aluminum Alloys (AA5052 & AA6061)

Chikkam Srikanth[a], *, Dr. R. Vaira Vignesh[a], **, and Dr. R. Padmanaban[a], ***

[a] Department of Mechanical Engineering, Amrita School of Engineering, Coimbatore, Amrita Vishwa Vidyapeetham, India
*e-mail: srikanth.chikkam@gmail.com
**e-mail: r_vairavignesh@cb.amrita.edu
***e-mail: dr_padmanaban@cb.amrita.edu

Abstract—Friction stir welding is one of the promising techniques to join dissimilar aluminum alloys. In this study, the friction stir welding technique is implemented to enable a sound butt-joint between aluminum alloy AA5052 and AA6061. The study investigates the influence of conventional heat treatment and newly-devised cyclic treatment on the properties of the friction stir weldment. The results indicate that the newly-devised cyclic heat treatment increases the microhardness by ~22%, tensile strength by ~22%, and ductility by 20% than the conventionally heat-treated specimens. The mechanism of property enhancement in the weldment is comprehensively correlated with the microstructural evolution.

INTRODUCTION

Aluminum and its alloys are the most used and the most demanded metallic material systems. Aluminum alloys are lightweight, non-toxic, corrosion-resistant, electrically and thermally conductive, and characterized by high formability, high reflectivity, good recyclability, and good strength-to-weight ratio. The requirement for joining aluminum alloys is augmented day by day for lightweight frames and structural applications [1]. Hence, aluminum alloys are mostly used in aerospace, defense, and automobile applications [2]. In such applications, the joining of components is indispensable. The joining of components that are made of dissimilar materials could be achieved by mechanical fastening and welding methods. However, the high oxidation tendency limits the possibility of joining aluminum alloy-based components by conventional welding technique. Hence, novel solid-state welding techniques are preferred for conjoining aluminum alloy components (similar or dissimilar grades of aluminum alloy).

Friction Stir Welding (FSW) is one of the most reliable solid-state welding techniques [3]. Globally, researchers have been working to effectuate the FSW process for joining similar and dissimilar materials. FSW is executed by inserting the rotating FSW tool into the joint line of the workpiece under axial load, followed by the frictional translation. The simultaneous input of heat and stress causes plasticization of the materials. The formation, characteristics, and proper-ties of the zones in the FSW joint are influenced by the FSW parameters such as tool rotation speed, welding speed, tool geometry, and axial load [4]. Also, the relative positioning of dissimilar base materials on the advancing or the retreating side of the FSW tool influences the properties of the joint.

Karlsson et al., [5] optimized the FSW parameters for joining dissimilar aluminum alloys (AA5083 alloy & AA6082 alloy, Cu & AA5083 alloy, Al-clad AA2024 alloy & AA2024 alloy). The FSW trials were performed at a constant tool rotation speed and welding speed between 10 and 50 cm/min. The macroscopy revealed a ring structure in the nugget zone that in turn confirmed a homogenous mixing of materials. The microhardness of the nugget zone was lesser than the HAZ. The tensile strength increased with an increase in welding speed. Maximum tensile strength of 224 MPa was achieved in the specimen that was welded at 50 cm/min.

Filho et al., [6] optimized the FSW process parameters for joining dissimilar aluminum alloys (AA2024-T351 alloy & AA6056-T4 alloy) of 4 mm thickness. The FSW trials were performed at a constant rotation speed of 20 s^{-1} and welding speed between 0.7 and 3.3 mm/s. An increase in the welding speed decreased the stir zone size. Also, ineffective material flow caused kissing bond defects at high speeds. A minimum microhardness of 133 HV was observed at HAZ and a maximum microhardness of 152 HV was observed at the nugget zone. The tensile test results

confirmed that the FSWed specimen fractured in HAZ of AA2024 alloy, with a maximal strength of 423MPa. Khodir et al., [7] explored the dissimilar FSW of aluminum alloys (AA2024 alloy & AA7075 alloy) using an FSW tool of 12 mm shoulder diameter and 4 mm pin diameter. The FSW trials were performed with a rotation speed between 500 rpm and 1200 rpm, and welding speed between 150 mm/min and 400 mm/min. FSW of specimens at high welding speed resulted in pores and kissing bond defects. A minimum microhardness of 72 HV was observed at the HAZ region and a maximum microhardness of 157 HV at the nugget zone. The microhardness of the joint increased with an increase in welding speed. However, the maximum tensile strength of 246 MPa was observed in the specimens that were FSWed at low welding speeds.

Bahemmat et al., [8] optimized FSW process parameters for joining dissimilar aluminum alloys (AA6061-T6 alloy & AA7075-T6 alloy) of 5 mm thickness. The FSW trials were performed at a constant rotation speed of 900 rpm, the penetration depth of 0.3 mm, welding speed between 80 mm/min and 160 mm/min, and also changing the alloy in advancing side and retracting side. Macroscopy and microscopy of weld specimens revealed that tool geometry significantly contributed to heat generation and mixing of materials in the course of FSW. The dissolution of the strengthening precipitate $\beta11-Mg_5Si_6$ attributed to the decrease in hardness of the nugget zone than that of the base material. Besides, the joint strength was lower in the FSWed specimens that had low-strength alloy on the retracting side. Dinaharan et al., [9] optimized FSW process parameters for joining wrought and cast aluminum alloys (AA6061 alloy). The FSW trials were performed at a constant welding speed of 50 mm/min, an axial load of 8 kN, tool rotation speed between 800 rpm and 1400 rpm, and varying the advancing/retreating side material. The macrostructure analysis revealed that the percentage area occupied by advancing side alloy increases with an increase in tool rotation speed beyond 1000 rpm. The microstructural analysis confirmed the occurrence of the dynamic recrystallization phenomenon. The dissimilar joint exhibited a maximum tensile strength of 150 MPa when the cast aluminum alloy was placed on the advancing side and welded at a tool rotational speed of 1200 rpm. Tensile test evidenced the ductile fibrous fracture of the FSWed specimens.

Devaiah et al., [10] utilized FSW to join dissimilar aluminum alloys (AA5083-H321 alloy & AA6061-T6 alloy). FSW trials were performed at a constant transverse speed of 40 mm/min and tool rotation speed between 560 rpm and 1800 rpm. A maximum microhardness of 84 HV, tensile strength of 196 MPa, and impact strength of 29 J were observed in the specimen that was welded at 900 rpm, because of grain refinement. In all test results, a crest-parabolic trend was observed with an increment in tool rotation speed. Selamat et al., [11] analyzed the microstructural evo-lution and properties of FSWed similar aluminum alloys (AA5083 alloy) and dissimilar aluminum alloys (AA5083 alloy & AA6061 alloy). The welding trials were performed at 1000 rpm and 100 mm/min. Microstructural analysis revealed that microstructure was more abrupt on the advancing side than on the retreating side. Microhardness of 83 HV/74 HV was observed for similar/dissimilar alloys at the joint interface. Also, it was found that both the joints had a low hardness index in the nugget zone. Similarly, the tensile strength of FSWed similar alloy was greater than FSWed dissimilar alloys.

Park et al., [12] investigated the properties of FSWed dissimilar aluminum alloys (AA5052-H32 alloy & 6061-T6 alloy). The FSW trials were performed by changing the alloys on advancing and retreating sides and at a rotation speed of 2000 rpm and welding speed of 100 mm/min. The macrostructural showed the asymmetric shape of the nugget zone in the weldment of both the FSW trials. The microstructural analysis established that placing AA5052-H32 alloy on the advancing side encourages homogeneous mixing of alloys in the weldment. Consequently, a maximum tensile strength of 224 MPa was achieved in that specimen. The least microhardness was observed in the HAZ of AA5052-H32 alloy. Kumbhar et al., [13] performed FSW of dissimilar aluminum alloy (AA5052 alloy & AA6061 alloy) plates of 5 mm thickness with a rotation speed of 1120 and 1400 rpm, and welding speeds of 60, 80, and 100 mm/min. Maximum tensile strength of 225 MPa was measured in the specimen that was FSWed at 1400 rpm and 80 mm/min. The high tensile strength is attributed to the presence of a non-linear wavy pattern in the microstructure, which in turn indicated a homogeneous mixing of materials. Similar microhardness was observed in the nugget zone and HAZ.

Rajkumar et al., [14] performed FSW of dissimilar aluminum alloys (AA5052 alloy & AA6061 alloy) at a constant rotation speed of 710 rpm and welding speed of 20 and 28 mm/min using a threaded FSW tool. Macrostructure revealed a homogeneous mixing of two alloys in the weldment. However, small voids were formed at low welding speed. The microhardness of the joint was lower on the AA6061 alloy side. Maximum tensile strength of 180 MPa was recorded in the specimen that was FSWed at 710 rpm and 28 mm/min. The investigations concluded that a threaded tool is more effective than a conventional cylindrical tool.

Most of the research work on FSW of dissimilar aluminum alloy focus on the influence of process parameters on the microstructural evolution, microhardness, and, tensile strength of the joints. A few kinds of literature discuss the development of statistical models or soft-computing models for correlating the process parameters with the properties of the joint. Besides, the articles provided optimum process parameters to make defectless joints in FSWed dissimilar aluminum alloys with desirable properties. The influence of post-weld heat treatment on the micro-

Table 1. Chemical composition of AA5052 alloy and AA6061 alloy

Alloying elements	Si	Fe	Cu	Mn	Mg	Zn	Cr	Al
Chemical composition of AA5052 alloy (wt %)	0.072	0.340	0.038	0.056	2.546	0.010	0.178	96.767
Chemical composition of AA6061 alloy (wt %)	0.602	0.177	0.152	0.110	0.919	0.047	0.078	93.65

structural evolution and hence the properties of the joint are investigated by a handful of researchers across the world. Of which, most of the researchers followed conventional heat treatment procedures.

Elangovan et al., [15] analyzed the influence of post-weld solutionizing, post-weld aging, and combined post-weld solutionizing and aging heat treatment on the tensile strength of FSWed similar aluminum alloys (AA6061 alloy). The results indicate that the joint strength was weaker than the base material in the as-weld condition. The major precipitate in AA6061 alloy is Mg_2Si. The formation and distribution of these precipitates depend on solution treatment and aging treatment. Solution treatment followed by aging formed a supersaturated solid solution, beginning the precipitation of strengthening particles. In the artificially aged specimens, very fine precipitates are uniformly distributed throughout the matrix. This contributes to grain refinement in FSWed AA6061 alloy. The tensile strength was 20% higher than the base material. Besides, higher hardness of 102 Hv was observed. Priya et al., [16] examined the influence of post-weld solutionizing and post-weld aging treatment for similar and dissimilar FSWed aluminum alloys (AA2219 alloy and AA6061 alloy). The microstructural analysis revealed the refinement of grain structure after the heat treatment. The post-solutionizing treatment increased the hardness and tensile strength (312 MPa). However, the fracture mode was predominantly brittle. Hence, post-weld aging treatment was considered to be reasonably good for FSWed specimens. Similar results were achieved by Sivaraj et al., [17] in their research work on post-weld solutionizing and post-weld aging treatment for FSW of similar aluminum alloys of (AA7075 alloy). Microhardness and tensile strength (ductile character) were improved in the FSWed specimen after solutionizing treatment followed by aging.

Bayazid et al., [18] evaluated the performance of FSWed similar aluminum alloys (AA7075 alloy) that was subjected to cyclic heat treatment (400−480°C for 15 minutes). The results indicate a considerable grain refinement after cyclic heat treatment. The results explicit that the cyclic heat treatment improved tensile strength by 33% and hardness by 45%. The literature survey shows that most of the research work focused on the development of joints between dissimilar aluminum alloys utilizing FSW. Besides, a few research articles discuss the development of new cyclic heat treatments [18−24]. However, a comprehensive evaluation of the properties of conventional heat treatment and cyclic heat treatment (three cycles) is seldom discussed in the open literature. Many engineering applications in aerospace and automotive field require joining of dissimilar 5xxx to 6xxx aluminum alloys.

The primary objective of the research work is to determine the oprtimum FSW process window for conjoining AA5052 alloy & AA6061 alloy. The optimum FSW proces window would be determined based on macrostructure (defect-less) microstructure (refined grains), microhardness, and tensile strength. The secondary objective is the development of cyclic heat treatment cycle for improvising the properties (microstructure, microhardness, and tensile strength) of the FSWed joint.

OVERVIEW

In this study, the process window for obtaining defect-less FSW of AA5052 alloy & AA6061 alloy was determined. The following FSW process parameters were optimized to obtain defect-less welds: shoulder diameter, welding speed, and rotation speeds of the FSW tool. Further, the FSWed specimens were heat-treated following the conventional heat treatment cycle and the newly developed cyclic heat treatment cycle. The specimens were characterized for microstructural evolution and tested for microhardness, and tensile strength. The fractography analysis was performed to determine the fracture mechanism. Based on the metallurgical analysis and mechanical test results, the article comprehensively describes the optimum FSW process parameters and heat treatment cycle conjoining AA5052 alloy & AA6061 alloy.

MATERIALS AND METHODS

Chemical Composition of Alloys

The aluminum alloys used in the study were AA5052 alloy and AA6061 alloy. These alloys were tested for chemical composition using optical emission spectroscopy. The spectroscopy results of AA5052 alloy and AA6061 alloy are listed in Table 1. The results confirm that the weight percentage of alloying elements and compositional limit of the trace elements in AA5052 alloy and AA6061 alloy is in line with the ASTM E125:2011 standard.

Welding Machine and Tool Specifications

The FSW machine used for experimental trials is shown in Fig. 1a. The spindle gearbox consists of variable tool rotation speeds between 0 and 1400 rpm. The bed gearbox consists of variable speeds from 0 to
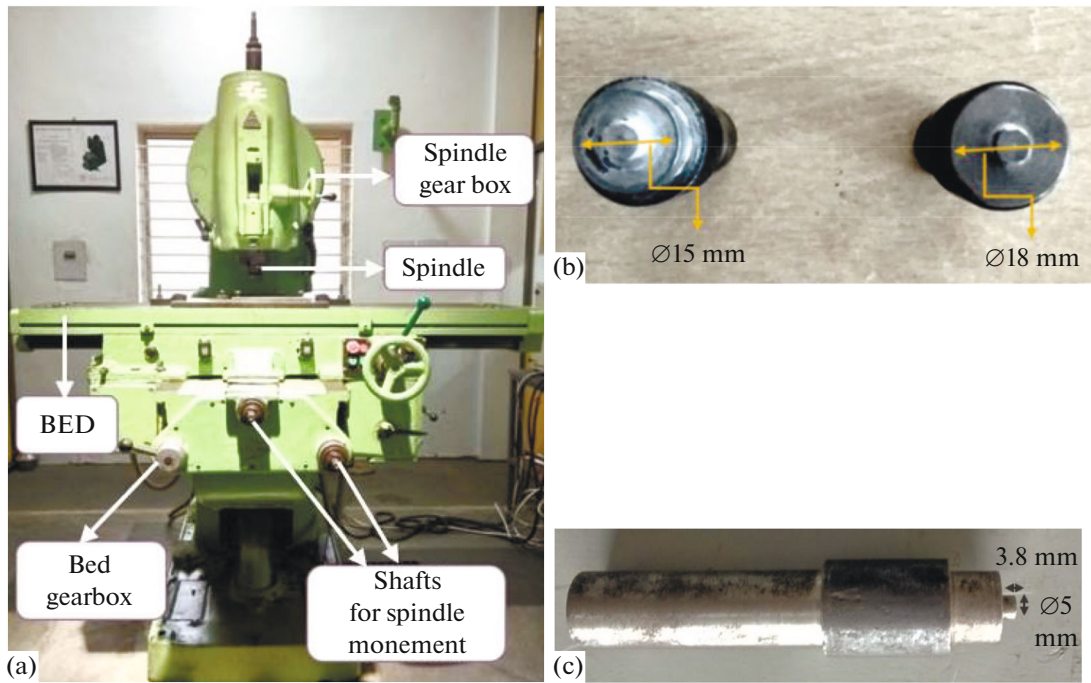
Fig. 1. (a) FSW Setup at Amrita Vishwa Vidyapeetham; (b) FSW tools—shoulder dimensions; (c) FSW tools—pin dimensions.

1250 mm/min. The variable speeds are controlled by an electronic control unit. The FSW tools are shown in Figs. 1b, 1c. The FSW tool material was High Carbon High Chromium steel (HCHCr). The geometrical aspects of the FSW tool are as follows:

(1) FSW Tool 1: Cylindrical tool pin; tool pin height 3.8 mm; tool pin diameter 5 mm; tool shoulder diameter 15 mm.

(2) FSW Tool 2: Cylindrical tool pin; tool pin height 3.8 mm; tool pin diameter 5 mm; tool shoulder diameter 18 mm.

Workpiece Preparation

The aluminum alloy (AA5052 alloy & AA6061 alloy) plates of dimension 180 mm length, 50 mm breadth and 4 mm width were used for experimentation. A cylindrical hole of 5 mm diameter was pre-drilled on the plates using a 5 mm diameter HSS drill at the interface of the plates using vertical drilling machines. The hole was drilled in such a way that a semicircular hole of diameter 2.5 mm was in each of the plates as shown in Fig. 2. The pre-drilled hole reduces the vibrations and the deviations of plates during plunging of the FSW tool into the workpiece at high rotation speeds.

Experimental Layout

The experimental trials were conducted by changing process parameters (rotation speed, welding speed, and shoulder diameter of the tool) to achieve defectless welded joints. The rotational speed of the tool var-

ied between 1000 and 1200 rpm. The welding speed was varied between 10 and 20 mm/min. The tool shoulder diameter was varied between 15 mm and 18mm. The penetration depth of the tool was varied as 3.8 mm (low), 3.9 mm (medium), and 4.0 mm (high) that was measured from the surface of the specimens. The experimental trials were performed as per the layout given in Table 2.

Macrostructure and Microstructure

The specimens for macrostructural and microstructural analysis were prepared and polished as per the outlines of the standard ASTM E3-11 [25]. The polishing was done using standard metallographic sheets (600, 800, 1000, 2000 grit) to obtain a mirror
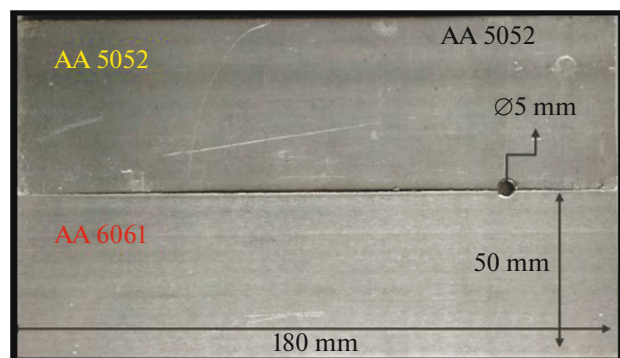
Fig. 2. FSW joint configuration—AA5052 alloy and AA6061 alloy.

Table 2. Experimental layout and specimen codes

Sl. no.	Specimen code	Tool rotation speed, rpm	Welding speed, mm/min	Tool shoulder diameter, mm	Penetration depth, mm
1	FSW01	1000	20	15	3.8
2	FSW02	1000	20	15	4.0
3	FSW03	1000	20	15	3.9
4	FSW04	1200	10	15	3.9
5	FSW05	1000	20	18	3.9
6	FSW06	1200	10	18	3.9

surface finish. The specimens were photographed using a high-resolution camera to observe macrostructural defects. The polished specimens were etched with modified Keller's reagent (180 mL of distilled water, 2 mL of HCl, and 5 mL of HNO$_3$) by referring to the ASM handbook. The polished specimens were etched by dipping for 20 s in etchant and rinsed in running water and acetone. Then the specimens were placed in the microscope (Make: Carl Zeiss; Model: Axiovert 25) and microstructure images were obtained at magnifications of 100×, 200×, and 500×.

Microhardness

The microhardness of the specimens was measured in the Mitutoyo Vicker's microhardness machine (Make: UHL; Model: VMHT 104) as per ASTM E92 standard under the axial load of 100 gf for 15 s. The diagonal indents (D1 and D2) were measured to determine the Vicker's microhardness of the specimens. The microhardness was taken in the regions of the nugget zone, TMAZ, and base material zone (AA5052 alloy and AA6061 alloy).

Tensile Test

Three sub-sized tensile samples inline with ASTM E-8M standards were prepared, as given in Fig. 3. (dimensions in mm). The uniaxial tensile test was performed in the tensile testing machine (Make: Tinus Olsen; Model: H25KT) at 0.5 mm/min crosshead speed.

Conventional Heat Treatment and Cyclic Heat Treatment

Conventional heat treatment was performed for the FSWed specimens at the aging temperature of heat treatable alloy (AA6061 alloy). The tensile specimens of base materials and weld materials were placed in the heating furnace at a temperature of 160°C for 18 hours as per the ASTM B917M standard [16]. The cyclic heat treatments were designed for the FSWed specimens, with three cycles namely C-1, C-2, and C-3. The cycle C-1 lasts for 6 hours at 160°C and cools down to room temperature (RT). In cycle C-2, cycle C-1 was repeated twice whereas, in cycle C-3, cycle C-1 was repeated thrice. The conventional heat treatment and cyclic heat treatment cycles are given in Figs. 4 and 5 respectively.

Fractography

The surface morphologies of the specimens of the tensile tests at the fracture region were observed using the field emission scanning electron microscope (Make: Zeiss Sigma). The fractographs were captured at 5 and 10 kV electron acceleration voltage and different magnifications to analyze the fractured surface and to determine fracture mode.

RESULTS AND DISCUSSIONS

FSW Trials and Optimization

The previous research work suggests the positioning of relatively softer alloys on the advancing side of the tool. Hence, the FSW trials were performed by
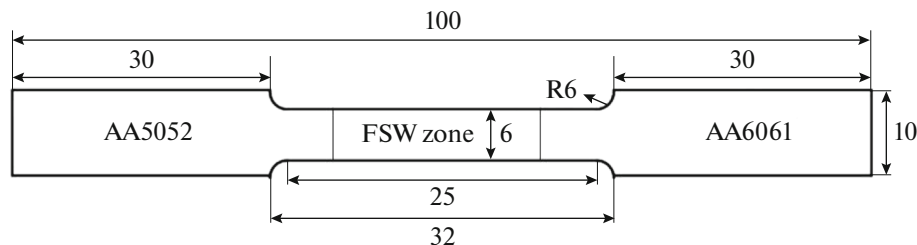
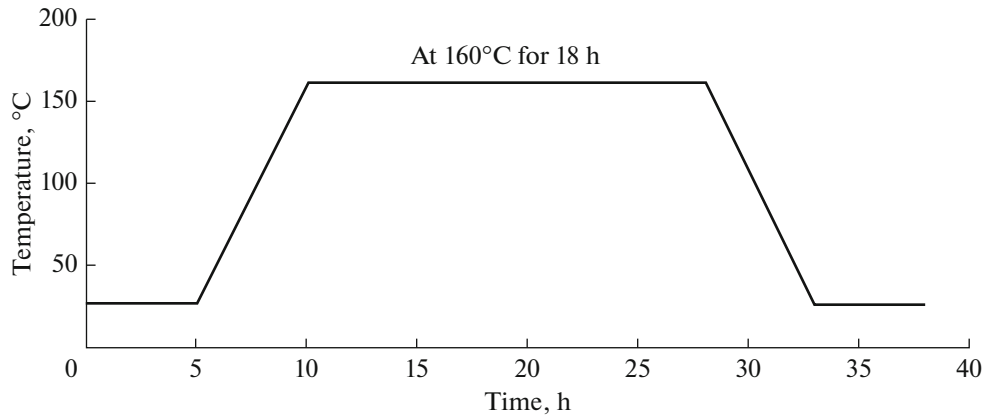**Fig. 3.** Schematic diagram of standard tensile specimen.

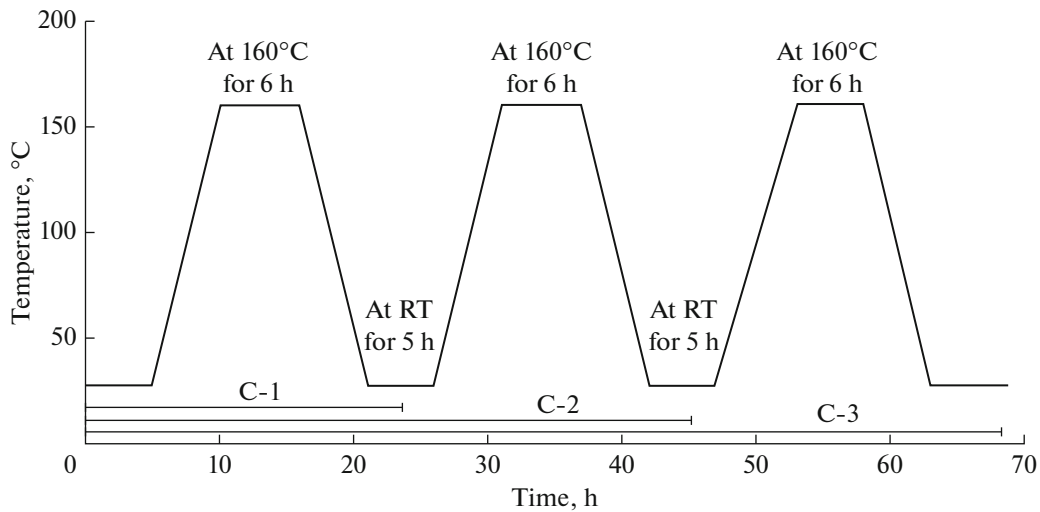**Fig. 4.** Conventional cyclic heat treatment.

Fig. 5. Cyclic heat treatment.

positioning AA5052 alloy on the advancing side and AA6061 alloy on the retreating side. Subsequently, FSW trials were performed by varying rotation speed, welding speed, and shoulder diameter of the tool. The photographs of the weldments with corresponding technical observations are presented in Table 3. In the trial FSW01, the workpieces were joined with a low tool penetration depth. The partial penetration of the tool negatively influenced the heat generation and hence resulted in improper joint.

In the trial FSW02, the plates were joined with high tool penetration depth. Because of high penetration depth, the workpiece deformed extensively. Hence, subsequent trials were performed with medium tool penetration depth (3.9 mm). In FSW03 and FSW04 trials, improper fusion was observed in the root region. The ineffective heat generation was attributed to the formation of defects in the weldments. Hence, the subsequent trials (FSW05 and FSW06) were performed with an FSW tool of shoulder diameter 18 mm. The trial FSW05 that was performed at 1000 rpm,

20 mm/min was observed to have a non-defective joint with the proper fusion of alloys. In the trial FSW06, workpieces were joined at high rotation speed (1200 rpm) and low welding speed (10 mm/min).

The high rotation speed caused the turbulent flow of highly plasticized materials and in turn, resulted in surface lack of fill. As the specimens FSW01 and FSW02 had externally visible defects and improper joining, they were not considered for macrostructure analysis. The macrostructure analysis of the specimens FSW03, FSW04, FSW05, and FSW06 are presented in the succeeding section.

Macrostructures of FSWed Specimens

The macrostructures and the technical observations of the specimens FSW03, FSW04, FSW05, and FSW06 trials are given in Table 4. In the figures shown in Table 4, the left side of the image was AA6061 alloy (retreating side) and the right side of the image was AA5052 alloy (advancing side). In the weld cross-sec-

Table 3. Technical observation of FSWed workpieces
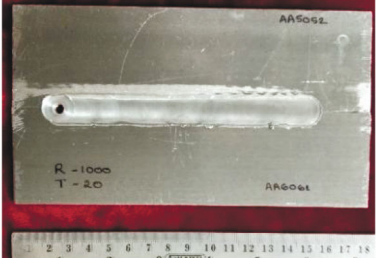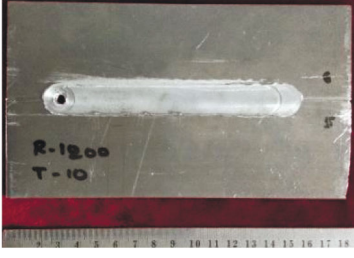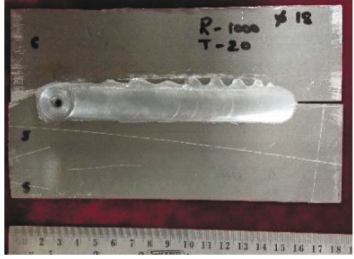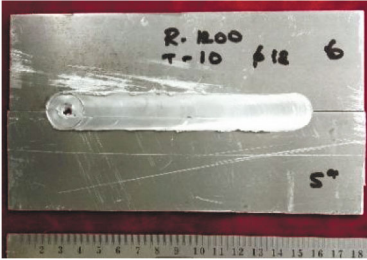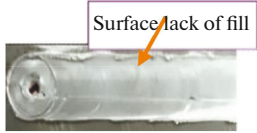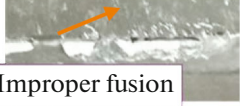
Sl. no.	Specimen code	Workpiece	Observation
1	FSW01		• Less depth of penetration
2	FSW02		• More depth of penetration • Plates tend to deform at the end
3	FSW03		• Improper fusion in the root region
4	FSW04		• Improper fusion of joints in the root region
5	FSW05		• No wormholes • Proper fusion of alloys
6	FSW06		Surface lack of fill Improper fusion

Table 4. Microstructures of FSWed specimens
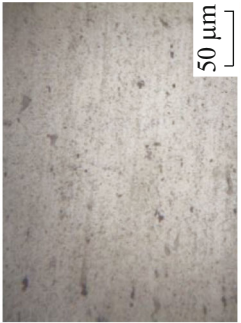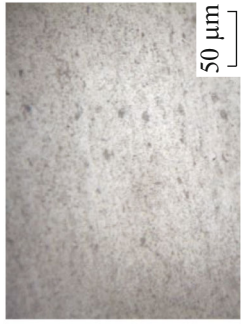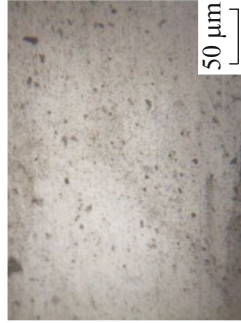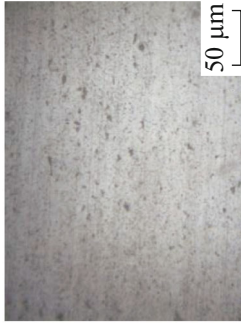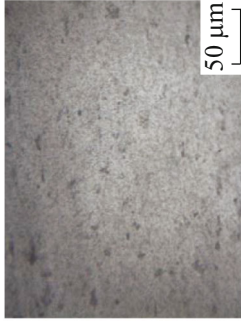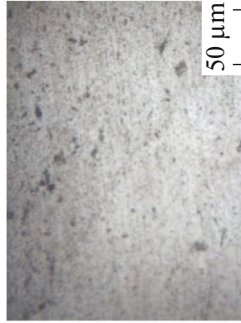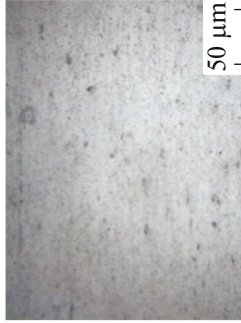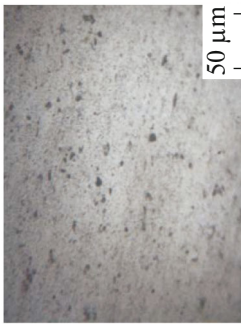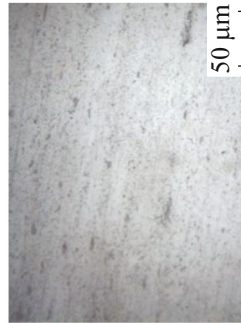
Sl. no.	Specimen code	AA5052 alloy base material	AA6061 alloy base material	Nugget zone	Defects
1	FSW03	50 μm	50 μm	50 μm	20 μm
2	FSW04	50 μm	50 μm	50 μm	20 μm
3	FSW05	50 μm	50 μm	50 μm	20 μm
4	FSW06	50 μm	50 μm	50 μm	20 μm

Table 5. Macrostructures of FSWed specimens

Sl. no.	Specimen code	Image	Observation
1	FSW03		Pinhole defect
2	FSW04		Wormhole defect
3	FSW05		No defect
4	FSW06		Pinhole defect

tion, the mechanically mixed and plasticized swirl flow of alloys (AA5083 alloy and AA6061 alloy) was observed. The alloy on the advancing side had occupied most of the region in the joint interface. The trial FSW03 and FSW06 exhibited pinhole defects that are attributable to the improper FSW parameters. In the FSW04 trial, a wormhole defect was observed. The specimen FSW05 was devoid of defects. However, specimens FSW03, FSW04, FSW05, and FSW06 were subjected to microstructural analysis to attest to the formation of defects.

Microstructures of FSWed Specimens

The microstructures of the specimens FSW03, FSW04, FSW05, and FSW06 are shown in Table 5. The microstructural analysis confirmed the defects (wormholes and pinholes) in the specimens FSW03, FSW04, and FSW06. The specimen FSW05 was confirmed defectless in the micron level of magnification. Thus, the tool rotation speed of 1000 rpm, welding speed of 20 mm/min, and the FSW tool with shoulder diameter of 18 mm were considered as optimum FSW process parameters for joining AA5052 alloy and AA6061 alloy of thickness 4 mm. Additional FSW trials at optimized parameters confirmed the repeatability of achieving defectless-weldment. The specimen FSW05 was considered for further investigations.

The microstructures of specimen FSW05 are given in Fig. 6. The FSW joint was bounded by unaltered base material on either side. Closer to the base material, heat affected zone (HAZ) was observed. Thermomechanically affected zone (TMAZ) was existent at the center of the FSW joints. The microstructure consisted of prominent regions such as AA5052 alloy base material, AA6061 alloy base material, and TMAZ on the AA5052 alloy side, and TMAZ on the AA6061 alloy side and nugget zone. The secondary intermetal-

lic phase in AA5052 alloy is Al−Mg (Al_3Mg_2) and AA6061 alloy is Al−Mg−Si (Mg_2Si). The dark spots in the microstructure indicate the respective intermetallic phases of AA5052 alloy and AA6061 alloy. The grains in the AA6061 alloy were coarser than the AA5052 alloy. Further, the grains in the TMAZ were slightly coarser than in the nugget zone. At the interface, the dark and bright color regions differentiate both the alloys. Besides, macrosegregation and microsegregation phenomena were not observed in the nugget zone.

In FSW, a rotating FSW tool was inserted into the joint line of the workpiece under axial load, followed by the frictional translation. The simultaneous input of heat and stress causes severe plastic deformation and plasticization of the materials in the vicinity of the joint line. Hence, multiple dislocations were induced in the nugget zone. The stirring action of the tool fragmented the secondary phases (Al_3Mg_2 and Mg_2Si) in the nugget zone. Also, the frictional heating results in partial dissolution of those secondary phases. The developed stresses and input frictional heat aided in dynamic recovery and recrystallozation of the nugget zone. Hence, the FSW joints were metallurgically characterized with fine grains, fragmented and submicron secondary phases. The grains in the base material were undisturbed that confirmed the optimum heat generation in the course of FSW. [14].

Conventional Heat Treatment and Cyclic Heat Treatment

Conventional heat treatment was performed at the aging temperature of the heat treatable alloy (AA6061 alloy). The tensile specimens of base materials and FSWed specimen (FSW05) were placed in the heating furnace at a temperature of 160°C for 18 h. The cyclic heat treatments were designed with three cycles
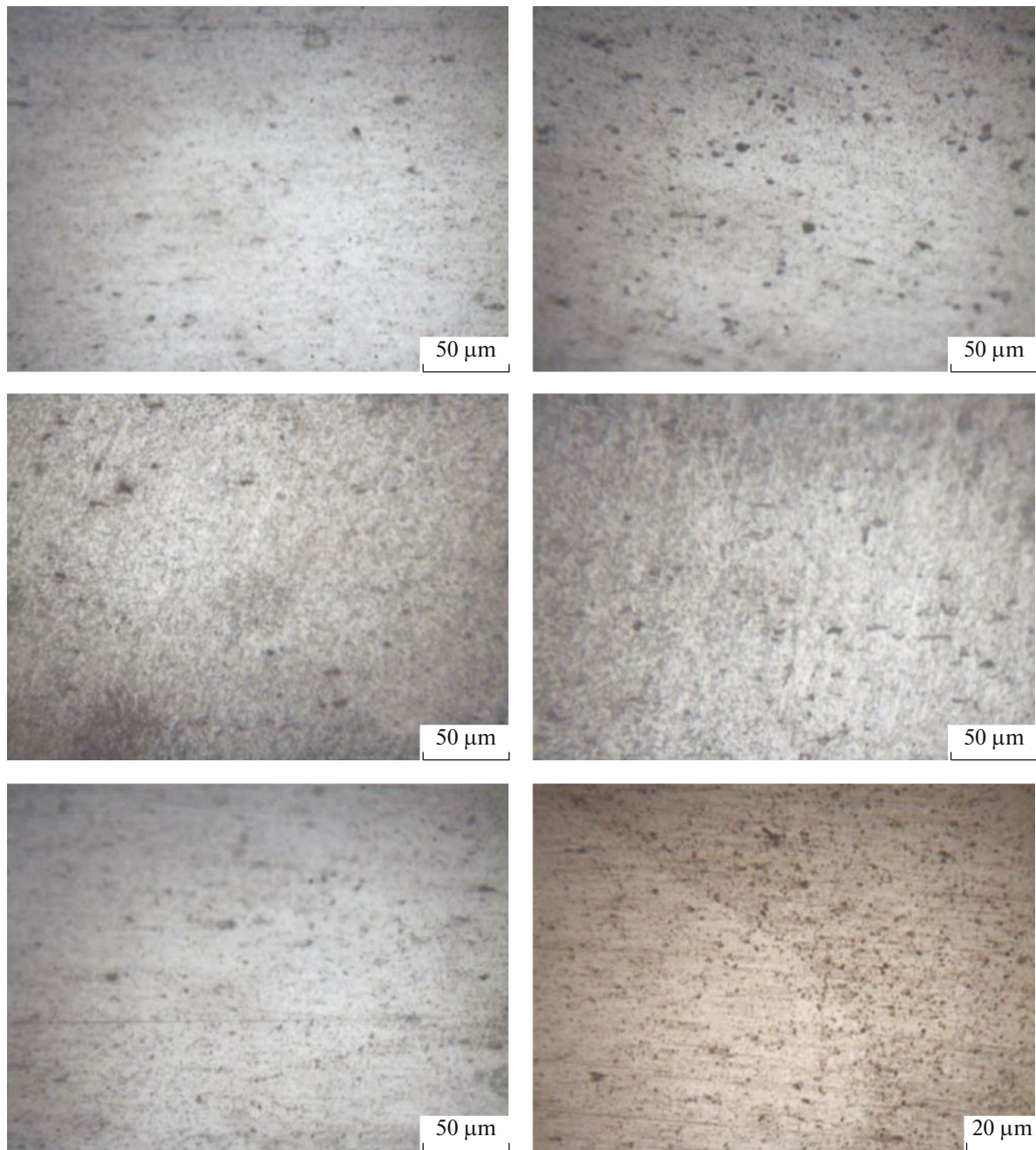
Fig. 6. Microstructure (a) BM AA5052 alloy (FSW05); (b) BM AA6061 alloy (FSW05); (c) TMAZ on AA5052 alloy side (FSW05); (d) TMAZ on AA6061 alloy side (FSW05); (e) Nugget zone (FSW05); (f) Nugget zone (FSW05).

namely C-1, C-2, and C-3. The cycle C-1 lasts for 6 h at 160°C and cools down to room temperature (RT). In cycle C-2, cycle C-1 was repeated twice whereas, in cycle C-3, cycle C-1 was repeated thrice. The fine intermetallic particles (strengthening precipitates) were formed during conventional heat treatment. The cyclic heat treatment resulted in the formation of finer strengthening precipitates than the conventional heat treatment. The formation of finer grains and homogeneous distribution of secondary intermetallic phase

particles in cyclic heat treatments influence the mechanical properties of the joints.

Microhardness of FSWed Specimens

The microhardness for as-welded, heat-treated, and cyclic heat-treated conditions are tested. In the TMAZ region, dissociation of intermetallic compounds resulted in a decrease in hardness. The increase in hardness at the nugget zone is the conse-
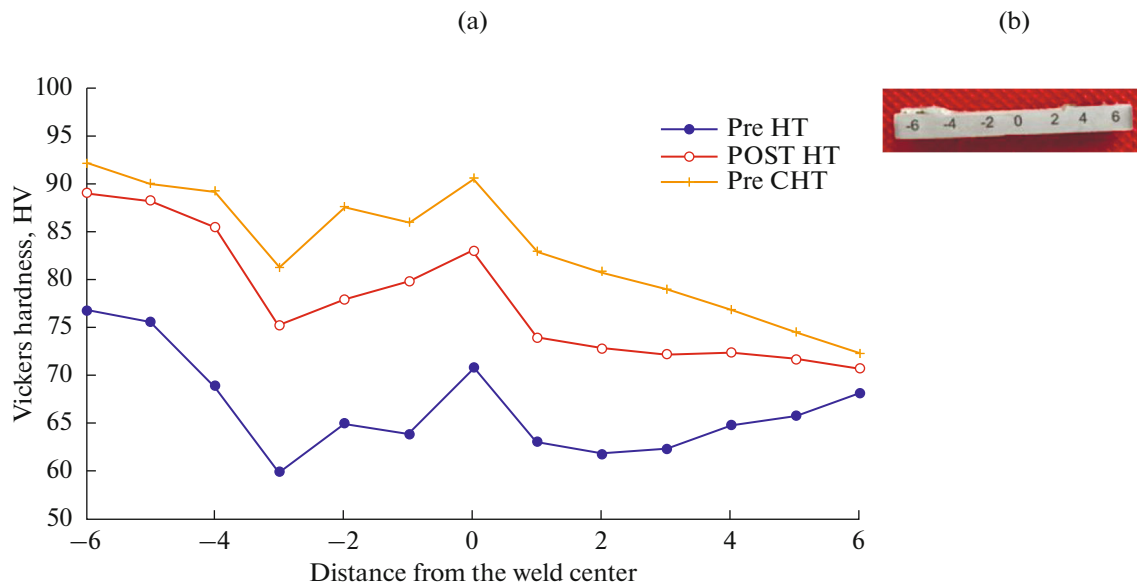
(a)   (b)

Fig. 7. (a) Microhardness of FSWed specimens; (b) plan of indentations.

quence of fine grain refinement caused by the effect of dynamic recrystallization and recovery. The microhardness of the specimens are given in Fig. 7a and the indentation locations are shown in Fig. 7b. The average microhardness in the nugget zone in the as-welded condition was 71 HV. After conventional heat treatment, the average microhardness in the nugget zone was 83.5 HV i.e. ~15% higher than the as-welded condition. After cyclic heat treatment (C-3), the average microhardness in the nugget zone was 91 HV i.e, ~22% higher than the as-welded condition and ~9% higher than the conventional heat-treated condition. After heat treatment and cyclic heat treatment, the increase in hardness is attributed to refinement in grains and fine dispersion of strengthening phases in the matrix, as described in the previous section.

Tensile Test of FSWed Specimens

The tensile tests were performed for the specimen FSW05 in as-welded, heat-treated, and cyclic heat-treated conditions, and results were compared with base materials. The specimens used for testing are shown in Fig. 8a. The specimens after tensile testing were shown in Figs. 8b−8f. All the tensile specimens failed at the TMAZ region of AA6061 alloy. As observed from the microhardness test, the microhardness of the specimen in TMAZ (fracture region) was lower than in other regions. In Fig. 8, AW represents the as-welded condition, C-1 represents cyclic heat treatment—1, C-2 represents cyclic heat treatment—2, C-3 represents cyclic heat treatment—3, and HT represents conventional heat treatment.

The typical uniaxial stress-strain graph is shown in Fig. 9a. The bar chart of the tensile strength of base materials and welded joints was shown in Fig. 9b. The bar chart of the percentage of elongation of base materials and welded joints was shown in Fig. 9c. The average tensile strength of the as-received AA5052 alloy was 261 MPa. The average tensile strength of the as-received AA6061 alloy was 322 MPa. The FSW05 specimen in as-welded condition had an average tensile strength of 147.3 MPa, which is 56% less than AA5052 alloy and 45.7% less than AA6061 alloy. After the conventional heat treatment, the specimen FSW05 had an average tensile strength of 170 MPa. This indicates that the average tensile strength of the specimen FSW05 improved by 13.4% after conventional heat treatment.

After the cyclic heat treatment C-1, the specimen FSW05 had an average tensile strength of 152.7 MPa. This indicates that the average tensile strength of the specimen FSW05 improved by 3.5% after cyclic heat treatment C-1. After the cyclic heat treatment C-2, the specimen FSW05 had an average tensile strength of 174.5 MPa. This indicates that the average tensile strength of the specimen FSW05 improved by 15.5% after cyclic heat treatment C-2. After the cyclic heat treatment C-3, the specimen FSW05 had an average tensile strength of 188.5 MPa.

This indicates that the average tensile strength of the specimen FSW05 improved by ~22% after cyclic heat treatment C-3. Hence, the cyclic heat treatment C-3 is recommended for maximizing the tensile properties of FSWed AA5052 alloy and AA6061 alloy. The percentage of elongation of welded joints is 59.14% less than that of AA5052 alloy and 54.73% less than that of AA6061 alloy. After conventional heat treatment, the percentage of elongation increased by ~4%

Fig. 8. (a) Tensile specimens; (b) AW specimens; (c) C-1 specimens; (d); (e) C-3 specimens; (f) HT specimens.
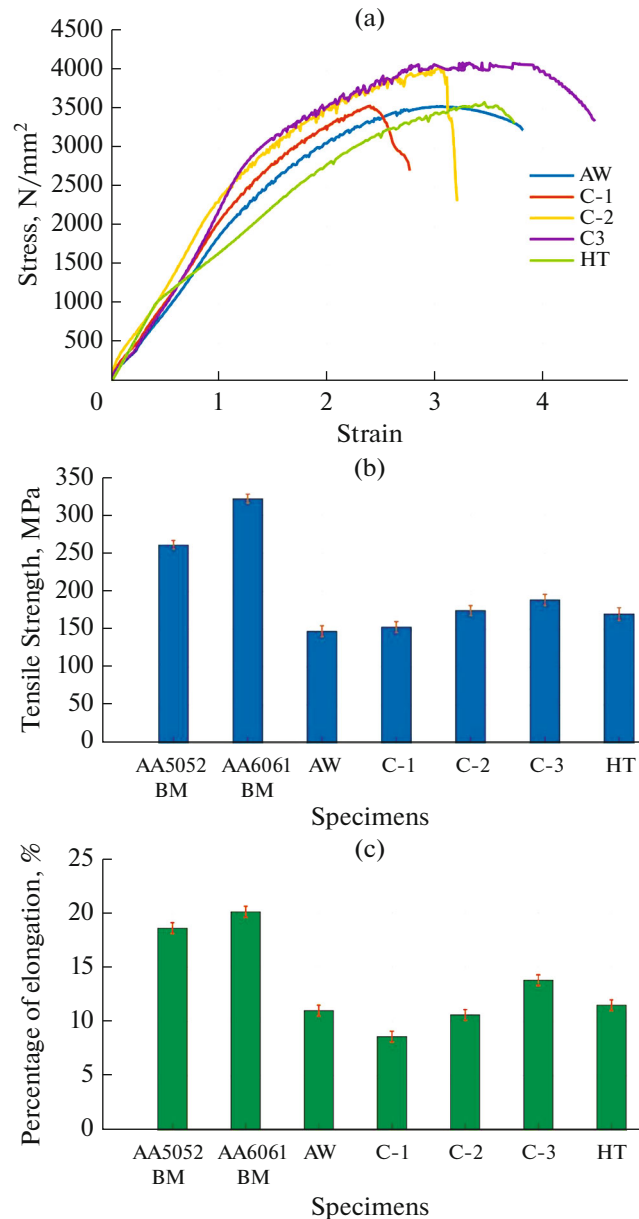
Fig. 9. (a) Stress-strain graph of specimens in all conditions (uniaxial tensile test); (b) tensile strength of base materials and welded joints; (c) percentage of elongation of the base materials and welded joints.

and after cyclic heat treatment (C-3), there was an increase of ~20%.

Fractography Analysis

The fractured surface morphology of the as-welded, heat-treated, heat-treated cycle 3 specimens was examined using a high-resolution scanning electron microscope. The fractographs of the as-welded specimen are shown in Fig. 10. The following features were observed in the fractographs: small deformation zone (shown in Fig. 10a), quasi-cleavage dimples (marked in Fig. 10b), and secondary cracks (marked in Figs. 10c, 10d). The presence of a small deformation zone confirms the low tensile strength of the joints. Besides, a few cleavage steps were observed on the fractured surface. Hence, the fracture mode was a combined ductile-brittle mechanism. The fractographs of the conventional heat treatment specimens are shown in Fig. 11.

The following features were observed in the fractographs: partial deformation zone (marked in Fig. 11b), intergranular fracture features, cracks, and secondary cracks (marked in Fig. 11c), and few cleavage steps (marked in Fig. 10d). The presence of a small deformation zone confirms the low tensile strength of the
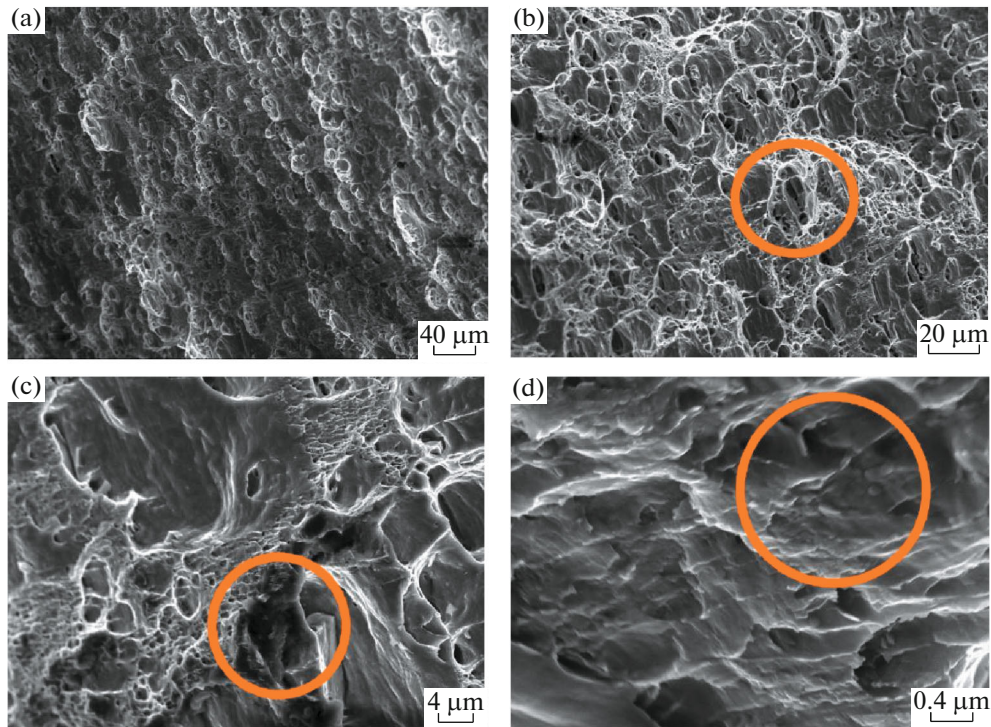
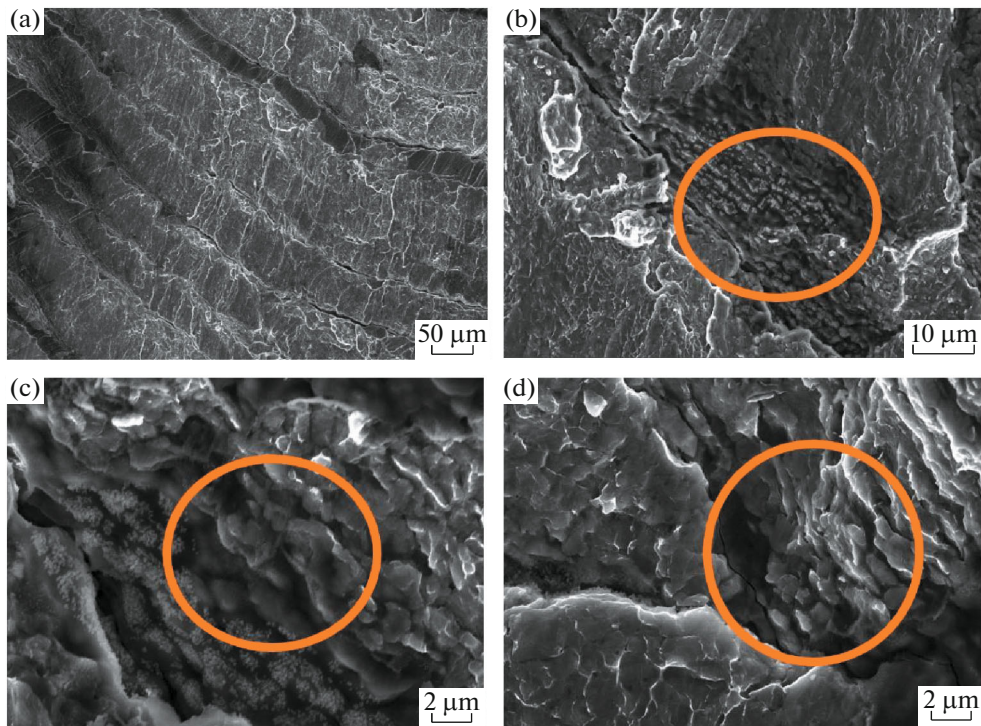**Fig. 10.** Fractograph of FSWed AW specimen.

Fig. 11. Fractograph of FSWed HT specimen.

joints. Also, a few cleavage steps were observed on the fractured surface. Hence, the fracture mode was a combined ductile-brittle mechanism. The fractographs of the specimen FSW05 subjected to cyclic heat treatment (C-3) are shown in Fig. 12. The following features are observed in the fractographs: large deformation zone (shown in Figs. 12a, 12d), secondary cracks (marked in Fig. 12c), and dimples (marked in Fig. 12b). The presence of a large deformation zone confirms the high tensile strength of the joints.
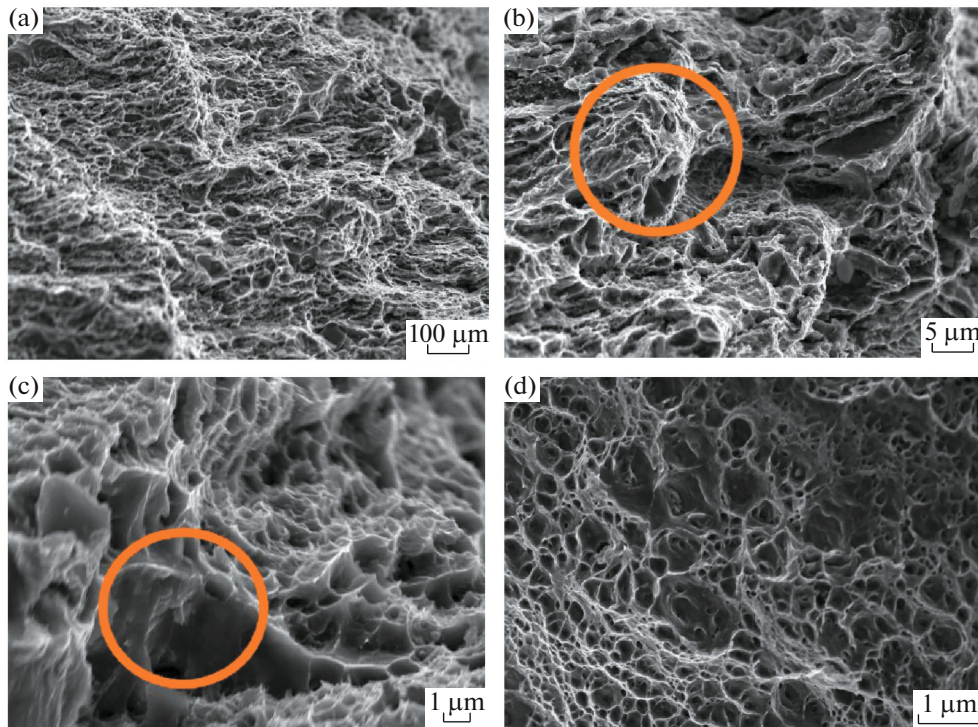
Fig. 12. Fractograph of the FSWed C-3 specimen.

Besides, quasi- cleavage dimples were observed on the fractured surface. Hence, the fracture mode was predominantly ductile natured. The fractography confirms the claims presented (tensile strength and ductility) in the previous section.

CONCLUSIONS

Friction stir welding of dissimilar aluminum alloys (AA5052 alloy & AA6061 alloy) was performed effectively. Conventional heat treatment and cyclic heat treatment cycles were designed and were performed successfully. The results demonstrate the following:

(1) The microstructural analysis evidenced that grains in the AA6061 alloy were coarser than the AA5052 alloy. Further, the grains in the TMAZ were slightly coarser than in the nugget zone. Besides, macrosegregation and microsegregation phenomena were not observed in the nugget zone.

(2) Microhardness at the nugget zone was higher than the base material and TMAZ. The maximum microhardness of 91 Hv was obtained after the cyclic heat treatment (C-3). The microhardness was increased by ~15% after conventional heat treatment whereas ~22% increase after cyclic heat treatment (C-3).

(3) The maximum tensile strength of the weld joints was 188.5 MPa after cyclic heat treatment (C-3). The tensile strength of the weld joint was increased by ~22% after cyclic heat treatment, whereas conventional heat treatment increased by ~13% only. The

ductility of the joint was increased after cyclic heat treatment (C-3).

that he/she has full power to make this grant. The author signs for and accepts responsibility for releasing this material on behalf of any and all co-authors. This transfer of publication rights covers the non-exclusive right to reproduce and distribute the article, including reprints, translations, photographic reproductions, microform, electronic form (offline, online), or any other reproductions of similar nature.

REFERENCES

1. Ramalingam, V.V., Ramasamy, P., Kovukkal, M.D., and Myilsamy, G., Research and development in magnesium alloys for industrial and biomedical applications: A review, *Met. Mater. Int.,* 2019, pp. 1–22. Ramalingam, V.V., Ramasamy, P., Kovukkal, M.D., and Myilsamy, G., Research and development in magnesium alloys for industrial and biomedical applications: a review, *Met. Mater. Int.,* 2020, vol. 26, pp. 409–430.

2. Paidar, M., Vignesh, R.V., Khorram, A., Oladimeji Ojo, O.O., Rasoulpouraghdam, A., and Pustokhina, I., Dissimilar modified friction stir clinching of AA2024-AA6061 aluminum alloys: Effects of materials positioning, *J. Mater. Res. Technol.,* 2020, vol. 9, no. 3, pp. 6037–6047.

3. Raghav, A.K., Vignesh, R.V., Kalyan, K.P., and M. Govindaraju, Friction welding of cast iron and phosphor bronze, *J. Inst. Eng. (India): Ser. C,* 2020, vol. 101, pp. 347–354.

4. Padmanaban, R., Balusamy, V., and Vaira Vignesh, R., Effect of friction stir welding process parameters on the tensile strength of dissimilar aluminum alloy AA2024-T3 and AA7075-T6 joints, *Materialwiss. Werkstofftech.,* 2020, vol. 51, no. 1, pp. 17–27.

5. Karlsson, L., Berqvist, E.-L., and Larsson, H., Application of friction stir welding to dissimilar welding, *Weld. World,* 2002, vol. 46, nos. 1–2, pp. 10–14.

6. Amancio-Filho, S., Sheikhi, S., Dos Santos, J., and Bolfarini, C., Preliminary study on the microstructure and mechanical properties of dissimilar friction stir welds in aircraft aluminium alloys 2024-T351 and 6056-T4, *J. Mater. Process. Technol.,* 2008, vol. 206, nos. 1–3, pp. 132–142.

7. Khodir, S.A. and Shibayanagi, T., Friction stir welding of dissimilar AA2024 and AA7075 aluminum alloys, *Mater. Sci. Eng., B,* 2008, vol. 148, nos. 1–3, pp. 82–87.

8. Bahemmat, P., Haghpanahi, M., Besharati, M., Ahsanizadeh, S., and Rezaei, H., Study on mechanical, micro-, and macrostructural characteristics of dissimilar friction stir welding of AA6061-T6 and AA7075-T6, *Proc. Inst. Mech. Eng., Part B,* 2010, vol. 224, no. 12, pp. 1854–1864.

9. Dinaharan, I., Kalaiselvan, K., Vijay, S., and Raja, P., Effect of material location and tool rotational speed on microstructure and tensile strength of dissimilar friction stir welded aluminum alloys, *Arch. Civ. Mech. Eng.,* 2012, vol. 12, no. 4, pp. 446–454.

10. Devaiah, D., Kishore, K., and Laxminarayana, P., Effect of material location and tool rotational speed on the mechanical properties of dissimilar friction stir welded aluminum alloys (5083-H321 to 6061-T6), *Bonfring Int. J. Ind. Eng. Manage. Sci.,* 2016, vol. 6, no. 4, pp. 186–190.

11. Selamat, N.F.M., Baghdadi, A., Sajuri, Z., and Kokabi, A., Friction stir welding of similar and dissimilar aluminium alloys for automotive applications, *Int. J. Automot. Mech. Eng.,* 2016, vol. 13, p. 3401.

12. Park, S.-K., Hong, S.-T., Park, J.-H., Park, K.-Y., Kwon, Y.-J., and Son, H.-J., Effect of material locations on properties of friction stir welding joints of dissimilar aluminium alloys, *Sci. Technol. Weld. Joining,* 2010, vol. 15, no. 4, pp. 331–336.

13. Kumbhar, N. and Bhanumurthy, K., Friction stir welding of Al 5052 with Al 6061 alloys, *J. Metall.,* 2012, vol. 2012, article no. 303756.

14. RajKumar, V., VenkateshKannan, M., Sadeesh, P., Arivazhagan, N. and Ramkumar, K.D., Studies on effect of tool design and welding parameters on the friction stir welding of dissimilar aluminium alloys AA 5052–AA 6061, *Procedia Eng.,* 2014, vol. 75, pp. 93–97.

15. Elangovan, K. and Balasubramanian, V., Influences of post-weld heat treatment on tensile properties of friction stir-welded AA6061 aluminum alloy joints, *Mater. Charact.,* 2008, vol. 59, no. 9, pp. 1168–1177.

16. Priya, R., Effect of post weld heat treatment on the microstructure and tensile properties of dissimilar friction stir welded AA 2219 and AA 6061 alloys, *Trans. Indian Inst. Met.,* 2009, vol. 62, no. 1, pp. 11–19.

17. Sivaraj, P., Kanagarajan, D., and Balasubramanian, V., Effect of post weld heat treatment on tensile properties and microstructure characteristics of friction stir welded armour grade AA7075-T651 aluminium alloy, *Def. Technol.,* 2014, vol. 10, no. 1, pp. 1–8.

18. Bayazid, S.M., Farhangi, H., Asgharzadeh, H., Radan, L., Ghahramani, A., and Mirhaji, A., Effect of cyclic solution treatment on microstructure and mechanical properties of friction stir welded 7075 Al alloy, *Mater. Sci. Eng., A,* 2016, vol. 649, pp. 293–300.

19. Fathy, N., Ramadan, M., Hafez, K., Alghamdi, A., and Halim, K.A., Microstructure and induced defects of 6061 Al alloy after short times cyclic semi-solid heat treatment, *MATEC Web Conf.,* 2016, vol. 67, p. 05012.

20. Khludkova, A. and Savitskii, K., Effect of quenching temperature on pore formation during the cyclic heat treatment of aluminum, *Sov. Phys. J.,* 1965, vol. 8, no. 6, pp. 19–22.

21. Mahmood, N.Y., Zainulabdeen, A.A., Mohmmed, J.H., and Abd Oun, H., Effect of cyclic heat treatment on microstructure and mechanical properties of AA 6061-T6 aluminum alloy, *Al-Nahrain J. Eng. Sci.,* 2020, vol. 23, no. 4, pp. 383–387.

22. Mishra, S., Mishra, A., Show, B.K., and Maity, J., Simultaneous enhancement of ductility and strength in AISI 1080 steel through a typical cyclic heat treatment, *Mater. Sci. Eng., A,* 2017, vol. 688, pp. 262–271.

23. Omori, T., et al., Abnormal grain growth induced by cyclic heat treatment, *Science,* 2013, vol. 341, no. 6153, pp. 1500–1502.

24. Sui, S.-H., Song, T.-G., and Zhao, H.-Y., Cyclic heating treatment for microstructures evolution of LC9 aluminum alloy (J), *Foundry,* 2007, vol. 56, no. 2, pp. 10–13.

25. Vignesh, R.V., Padmanaban, R., Govindaraju, M., and Priyadharshini, G.S., Mechanical properties and corrosion behaviour of AZ91D-HAP surface composites fabricated by friction stir processing, *Mater. Res. Express,* 2019, vol. 6, no. 8, p. 085401.